Photoacoustics 6 (2017) 16–25

Contents lists available at ScienceDirect

Photoacoustics

journal homepage: www.elsevier.com/locate/pacs

Photoacoustic *in vitro* flow cytometry for nanomaterial research

Dmitry A. Nedosekin[a,*], Tariq Fahmi[b,c], Zeid A. Nima[d], Jacqueline Nolan[a], Chengzhong Cai[a,c], Mustafa Sarimollaoglu[a], Enkeleda Dervishi[e], Alexei Basnakian[b,f], Alexandru S. Biris[d], Vladimir P. Zharov[a]

[a] Arkansas Nanomedicine Center, University of Arkansas for Medical Sciences, Little Rock, AR 72205, United States
[b] Department of Pharmacology and Toxicology, University of Arkansas for Medical Sciences, Little Rock, AR 72205, United States
[c] National Toxicology Research Center, U.S. Foods and Drug Administration, Jefferson, AR 72132, United States
[d] Center for Integrative Nanotechnology Sciences, University of Arkansas at Little Rock, Little Rock, AR 72204, United States
[e] Center for Integrated Nanotechnologies, Los Alamos National Laboratory, Los Alamos, NM 87544, United States
[f] Central Arkansas Veterans Healthcare System, Little Rock, AR 72205, United States

ARTICLE INFO

Article history:
Received 29 September 2016
Received in revised form 31 January 2017
Accepted 14 March 2017

Keywords:
Photoacoustic
Flow cytometry
Nanotoxicity
Graphene
Gold nanorods

ABSTRACT

Conventional flow cytometry is a versatile tool for drug research and cell characterization. However, it is poorly suited for quantification of non-fluorescent proteins and artificial nanomaterials without the use of additional labeling. The rapid growth of biomedical applications for small non-fluorescent nanoparticles (NPs) for drug delivery and contrast and therapy enhancement, as well as research focused on natural cell pigments and chromophores, demands high-throughput quantification methods for the non-fluorescent components. In this work, we present a novel photoacoustic (PA) fluorescence flow cytometry (PAFFC) platform that combines NP quantification though PA detection with conventional *in vitro* flow cytometry sample characterization using fluorescence labeling. PAFFC simplifies high-throughput analysis of cell-NP interactions, optimization of targeted nanodrugs, and NP toxicity assessment, providing a direct correlation between NP uptake and characterization of toxicity markers for every cell.

1. Introduction

Understanding the interactions between nanomaterials and cells is becoming increasingly important due to the rapid growth of biomedical research focused on the use of various nanoparticles (NPs) as drug delivery vehicles and imaging and therapy enhancers [1–4]. A variety of NP characteristics, including structure, surface chemistry, and physical properties, dramatically affects cell-NP interactions [3–7]. Recent nanotechnology advances in diagnosis and targeting of tumors, especially circulating tumor cells (CTCs) *in vitro* [8,9] and *in vivo* [10,11], have demonstrated that specificity and efficacy of cell targeting are essential for successful NP-assisted diagnosis and therapy [9,12,13]. However, traditional methods for the quantification of NPs at the single cell level have limited throughput (electron microscopy methods) [14], low sensitivity (light scattering detection) [15–17], and/or the inability to analyze low atomic weight elements (electron microscopy [2,18], mass spectroscopy) [1,19]. For fluorescent NPs, conventional flow cytometry (FC) [20,21] and microscopy [22,23] may provide high throughput cell counting, sorting, and quantification of nanomaterials [24]. However, current FC systems, though compatible with fluorescent NPs, are not suited well for non- or weakly-fluorescent materials due to their low sensitivity of absorption detection [24] and the significant scattering/auto-fluorescence of cell structures [17,24]. FC quantification of NPs in cells using light scattering has been reported for large gold nanorods [25], TiO_2 and ZnO particles [26,27], and some 80–100 nm gold nanoparticles [17]. The major drawback of light scattering detection is the rather low light scattering of NPs smaller than 100 nm [28] and the strong light scattering background of cell structures. This limits detection sensitivity, even under ideal static conditions (microscopy) [16]. Fluorescent labeling of non-fluorescent NPs using chemical attachment of fluorescent tags makes it possible to use conventional FC analysis for uptake quantification; [29] however, such chemical modifications may dramatically change NP properties, including *in vivo* toxicity and/or targeting specificity, and, thus, are not desirable in the analysis of an NP toxicity profile.

* Corresponding author.
E-mail address: DNedosekin@uams.edu (D.A. Nedosekin).

http://dx.doi.org/10.1016/j.pacs.2017.03.002

The high throughput quantification of non-fluorescent NPs, intrinsic cell chromophores, and pigments (*e.g.*, hemoglobin or melanin in melanoma cancer cells) [11,30–39] at a single cell level can be done using light absorption contrast as an alternative to fluorescent labeling. The level of absorption sensitivity required for NP detection is achievable using photoacoustic (PA) detection, which is based on detection of acoustic waves generated in the sample upon absorption of laser irradiation followed by non-radiative relaxation and sample heating (Fig. 1). PA contrast is common for most nanomaterials (including fluorescent quantum dots) [33], light-absorbing proteins, and dyes. PA detection can be performed in static conditions and in flow, even in the presence of significant light scattering and auto-fluorescent backgrounds [37,40,41]. We previously demonstrated high-speed PA detection in flow as well as the feasibility of PA detection for various NPs, including single cells and NPs at flow velocities up to 3 m/s [11,35,40]. PA detection of cells and NPs has also been demonstrated in mouse blood [11,34,35], lymph [42], tomato plants [43], and artificial vessels [35]. The PA phenomenon demonstrates remarkable spectral selectivity [36], high sensitivity (single particle level) [31,33], and label-free absorbance quantification [11,37]. Still, full integration of PA technology into conventional flow cytometry has not been reported yet. Current PA detection in flow either lacks speed (*e.g.*, 10–20 Hz laser pulse repetition rate, PRR) [41,44,45] or does not provide multimodal (scattering, fluorescence, absorbance) analysis of single cells in fast flow [30,37,46].

Here, we report on the development of an integrated *in vitro* PA-fluorescence flow cytometry technique (PAFFC) that extends the range of application of conventional FC, allowing highly sensitive absorbance quantification and single NP detection sensitivity. PA detection serves as an additional source of data for complete cell characterization without compromising conventional fluorescence and light scattering detection of various cell biomarkers.

2. Materials and methods

2.1. PAFFC

The PAFFC system was built on the basis of an upright microscope (Nikon Eclipse E400, Nikon Instruments, Inc., Melville, NY, USA) with an acoustic transducer (V316-SM, 20 MHz, 12 mm focal distance, 150 μm focal area, Olympus) mounted over flow cells on an XY positioning stage (Fig. 2). The flow module of the cytometer was built using a quartz capillary (Molex Inc., Phoenix, AZ) with a 100 × 100 μm square cross-section placed on the bottom of a water-filled chamber. The microscope condenser was replaced with a custom laser delivery and fluorescence collection optics featuring 20× micro-objective (PlanFluor, NA 0.4; Nikon Instruments, Inc.). The setup was equipped with an 820-nm diode-pumped pulsed laser (PA excitation) with a maximal energy of 35 μJ, pulse duration of 8 ns, and pulse rate of 10 kHz (LUCE 820, Bright Solutions, Italy). Fluorescence was excited using a continuous wave (cw) diode 488 nm laser (IQ1C45 (488-60) G26, Power Tech., Alexander, AR, USA) having 7 mW power in the sample. Laser beams were shaped using cylindrical lenses and focused inside the capillary. Both lasers formed 5 × 150 μm lines across the main capillary axis. Fluorescence was collected through the same objective and separated from excitation light using several dichroic mirrors and a bandpass filter (FF01-520/15, Semrock Inc., Rochester, NY). A photomultiplier tube (R3896, Hamamatsu Co., Bridgewater, NJ) connected to a high-voltage pre-amplifier (C6271, DC to 10 kHz bandwidth, Hamamatsu Co., Bridgewater, NJ) was used to measure the intensity of collected fluorescent light. PA signals from the transducer were amplified (preamplifier 5678; bandwidth, 200 kHz–40 MHz; gain 40 dB; Panametrics NDT) and digitized (PCI-5124, 12-bit, 200 MSPS, National Instruments Inc.). Custom-developed software recorded amplitudes of PA signals for each laser pulse, along with the second channel data for photomultiplier tube signal voltage. Both traces were displayed in real time and saved for later off-line peak detection and other statistical analysis. All the data acquisition and analysis were performed using custom LabView-based software.

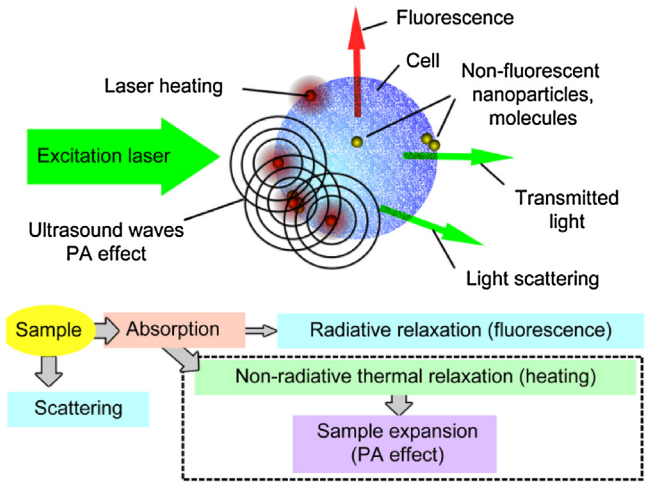

Fig. 1. Interaction of light with cells, NPs, chromo- and fluorophores, and corresponding phenomena.

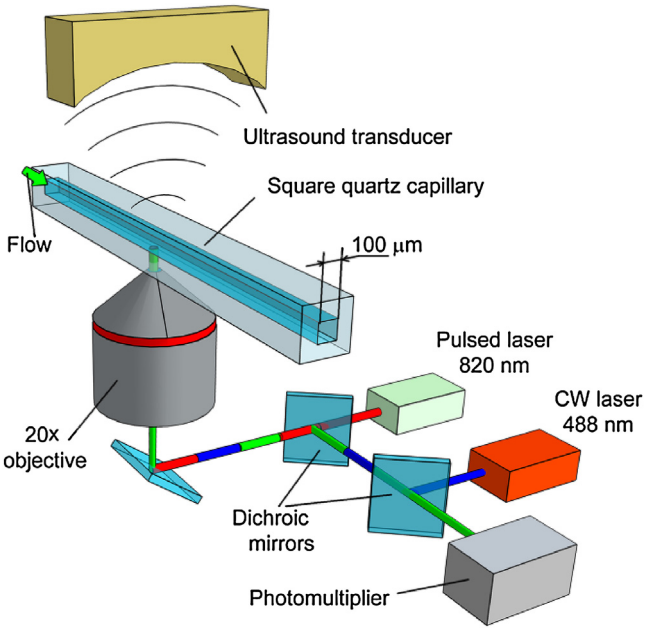

Fig. 2. General schematics of PAFFC system.

2.2. Enhanced dark-field microscopy

Dark-field imaging (light scattering contrast) of cells incubated with NPs was performed using an enhanced illuminator, CytoViva 150 (CytoViva Inc., Auburn, AL), and Solarc 24W metal halide fiber light source (Welch Allyn, Skaneateles Falls, NY). Images were taken using a 100× objective (Olympus UPlanAPO fluorite, N.A. 1.35–0.55) with a high-resolution color camera (DP72, Olympus America Inc.).

2.3. Raman microscopy

Raman signatures were collected from graphene-incubated samples using a confocal Raman spectrometer (Horiba Jobin Yvon LabRam HR800, Edison, New Jersey) assembled with a diode laser (784 nm) and Olympus BX-51 microscope platform featuring 100× micro-objective and a Peltier-cooled CCD camera. The spectrometer also has a three-dimensional (x-y-z) automatic adjustable stage that maps Raman signals for a specific area, with a spatial resolution of 1 μm. The spectra were collected using 600-line/mm gratings at 8 s acquisition time. All the data were baselined, background-corrected, and then re-instructed using OriginLab software. For all measurements, the spectrometer was calibrated using the Si–Si Raman signal at 52 cm^{-1}.

2.4. Cell and sample preparation

2.4.1. Cells

MDA-MD-MB-231 (basal-like subtype) and ZR-75-1 (luminal-like subtype) breast cancer cell lines (ATCC, Manassas, VA 20110 USA) were used to demonstrate labeling with gold NPs. Cells were cultured in Dulbecco's Modified Eagle's Medium (DMEM) with 10% fetal bovine serum, 1% L-glutamine, 100 U/mL penicillin, and 11 μg/mL streptomycin. A suspension of cells in phosphate buffered saline (PBS) was prepared at a final cell concentration of 10^5/mL for incubation experiments. Rat kidney tubular epithelial NRK-52E cells (ATCC, Manassas, VA) were grown in DMEM (ATCC) supplemented with 5% fetal bovine sera at 5% CO_2/95% air in a humidified atmosphere at 37 °C, fed at intervals of 48–72 h, and used within 1 day after confluence. Cells were treated with different concentrations of graphene (1.5–50 μg/mL) followed by 24 h incubation, after which they were harvested, washed in PBS, fixed, and stained for the terminal deoxynucleotidyl transferase dUTP nick end labeling (TUNEL) assay using the *In Situ* Cell Death Detection Kit (Roche Diagnostics, Indianapolis, IN) according to the manufacturer's protocol.

2.4.2. Gold nanorods

Gold nanorods (GNRs) with a core size of 25 × 113 nm, absorption maximum of 850 nm, conjugated to anti-EpCAM and anti-folate antibodies, and covered with a nonreactive polymer (nonreactive control) were purchased from Nanopartz Inc. (Loveland CO, USA). All GNR solutions were kept at 4 °C in order to minimize clustering during storage.

PA detection of single GNRs was performed using an ultra-diluted solution of NPs. The stock solution of GNRs was diluted 10^6-fold to the 10^6 particles/mL concentration, ensuring that only single particles occupied volume of the laser beam (0.05 nL). We estimate that the probability of two particles occupying the same detection volume was $\sim 1 \times 10^{-3}$.

Quantification of GNR uptake by breast cancer cells was performed using the following procedures: 5 min of water sonication (Branson, Danbury, CT 06810, USA) of GNR solution was done, then 10^9 GNRs were introduced to 1 mL PBS suspension of 10^5 cells at 4 °C for 60 min. After incubation, cells were washed twice to remove excess GNRs by gentle centrifuge (1000 rpm) and resuspended in PBS, stained with a SYTO® 9 (Green Florescent Nucleic Acid Stain, Life Technologies, Grand Island, NY 14072,USA), and resuspended in 1 mL PBS for PAFFC analysis.

2.4.3. Graphene

Graphene material (1–1.2-nm thick flakes) was purchased from Angstron Materials Inc. (product number N002-PDR; Dayton, OH) and partially functionalized with COOH groups to improve dispersion in water (Supplementary Document S2). For Raman imaging, the NRK-52E cells incubated with 50 μg/mL of graphene

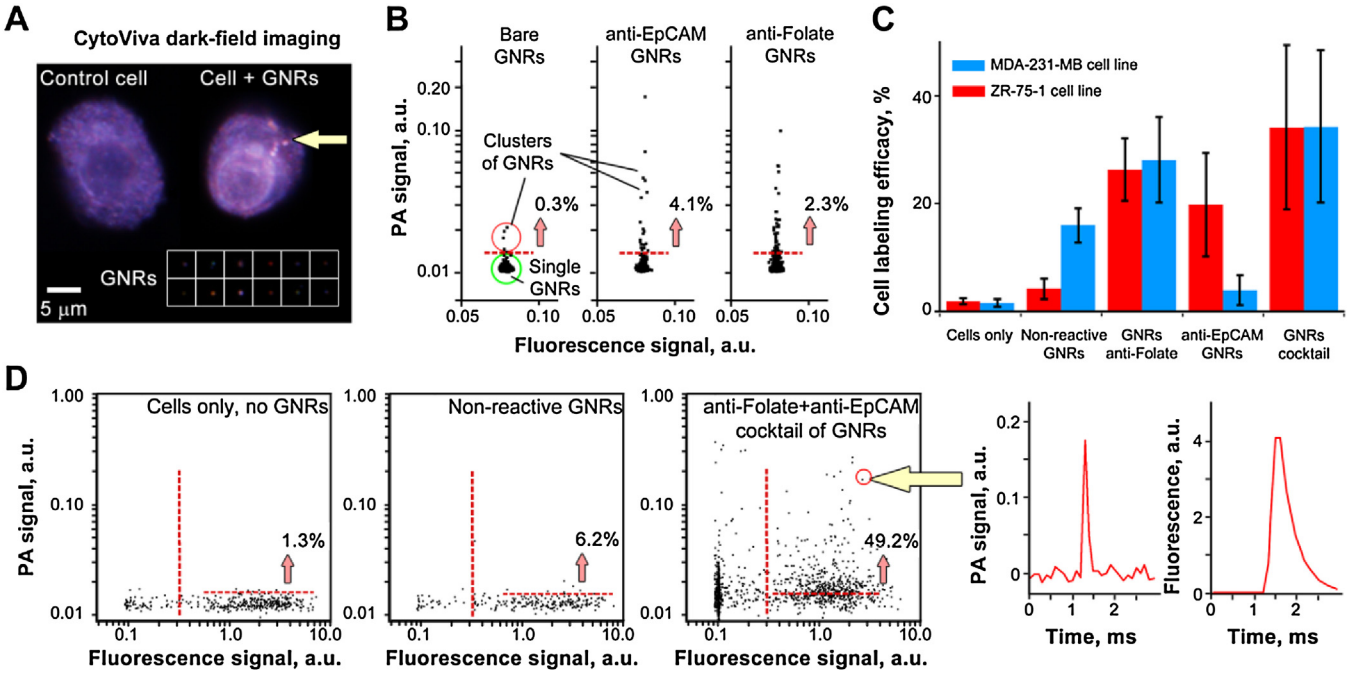

Fig. 3. PAFFC high-throughput assessment of cell-NP interactions: A) Enhanced dark-field imaging of a cell targeted by GNRs (CytoViva illuminator). The bottom panel illustrates typical dark-field signatures of GNRs in solution; arrows indicate presumed GNRs; B) PAFFC analysis of GNR solution (1:10^6 dilution). Fluorescence intensity of GNRs is at electronic noise level, $n = 3500$ in each plot; the horizontal threshold separates single particles (below) from clusters (above); C) PAFFC quantification of cell labeling efficiency for MDA-231-MB and ZR-75-1 breast cancer cells labeled with SYTO nucleic acid stain. Error bars show standard deviation for triplicate experiments. Number of cells in each experiment is 400–600; D) Typical 2D PAFFC plots for MDA-231-MB cells. Inset at right shows PA and fluorescence traces for one of the cells on a plot. Numbers on 2D plots indicate relative number of cells above the PA signal threshold (horizontal dash line: signal level set using PA signal for control cells without GNRs).

were sorted using the conventional Fluorescence Activated Cell Sorting (FACS, FacsAria) system. Sorted cells were analyzed by Raman microscope using glass-slide smears.

2.4.4. 2D PA-fluorescence scatterplots

PA/fluorescence data acquired by the PAFFC system were displayed as 2D scatterplots. The two axes represented PA (vertical axis) and fluorescence (horizontal axis) detectors. Each dot marked a single cell. Due to the absence of spectral overlap between PA and fluorescence signals, no compensation matrix was required. As is typical, two gates (threshold PA and fluorescence signals) were used to quantify cell populations. These gates formed four quadrants that correspond to four populations: high PA/low fluorescence (top left), high PA/high fluorescence (top right), low

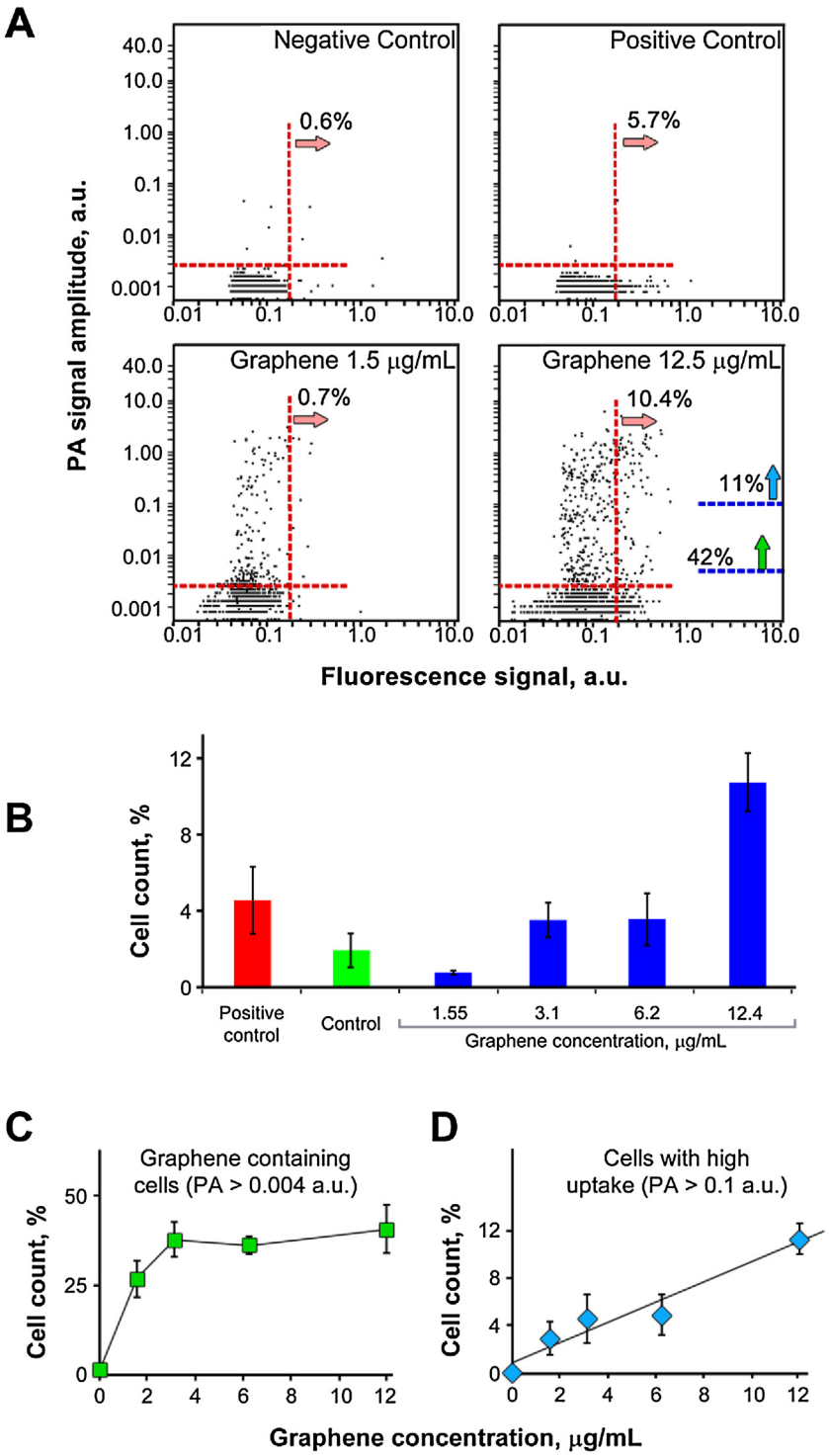

Fig. 4. PAFFC analysis of TUNEL staining and graphene uptake by NRK-52E rat kidney cells. A) 2D PAFFC charts correlating PA signal (graphene uptake) and fluorescence intensity (TUNEL staining) after 24 h incubation. Arrows indicate cell count over selected thresholds. B) Quantification of TUNEL-positive cells. C) Number of cells containing graphene (PA signals over 0.004 a.u.). D) Number of cells with high graphene uptake (PA signal over 0.1 a.u.). For B, C, and D, data is given as mean ± SD, triplicate experiments.

PA/high fluorescence (bottom right) and low PA/low fluorescence (bottom left). The relative number of cells in each quadrant was used to quantify changes taking place upon exposure of the cells to graphene. The fluorescence threshold was set up using control cell population; the PA threshold was set up using negative control (no NPs, PA signal defined by electronic noise). The numbers on the 2D plots show a relative number of cells having signals higher than a certain gate (as indicated by an arrow, Fig. 3D).

3. Results

3.1. High throughput quantification of cell labeling efficacy

The PAFFC system was used for rapid assessment of the efficacy of interactions between molecule-specific GNRs and MDA-231-MB-GFP and ZR-75-1 breast cancer cell lines in suspension. The interaction of GNRs with the cell membrane was confirmed by

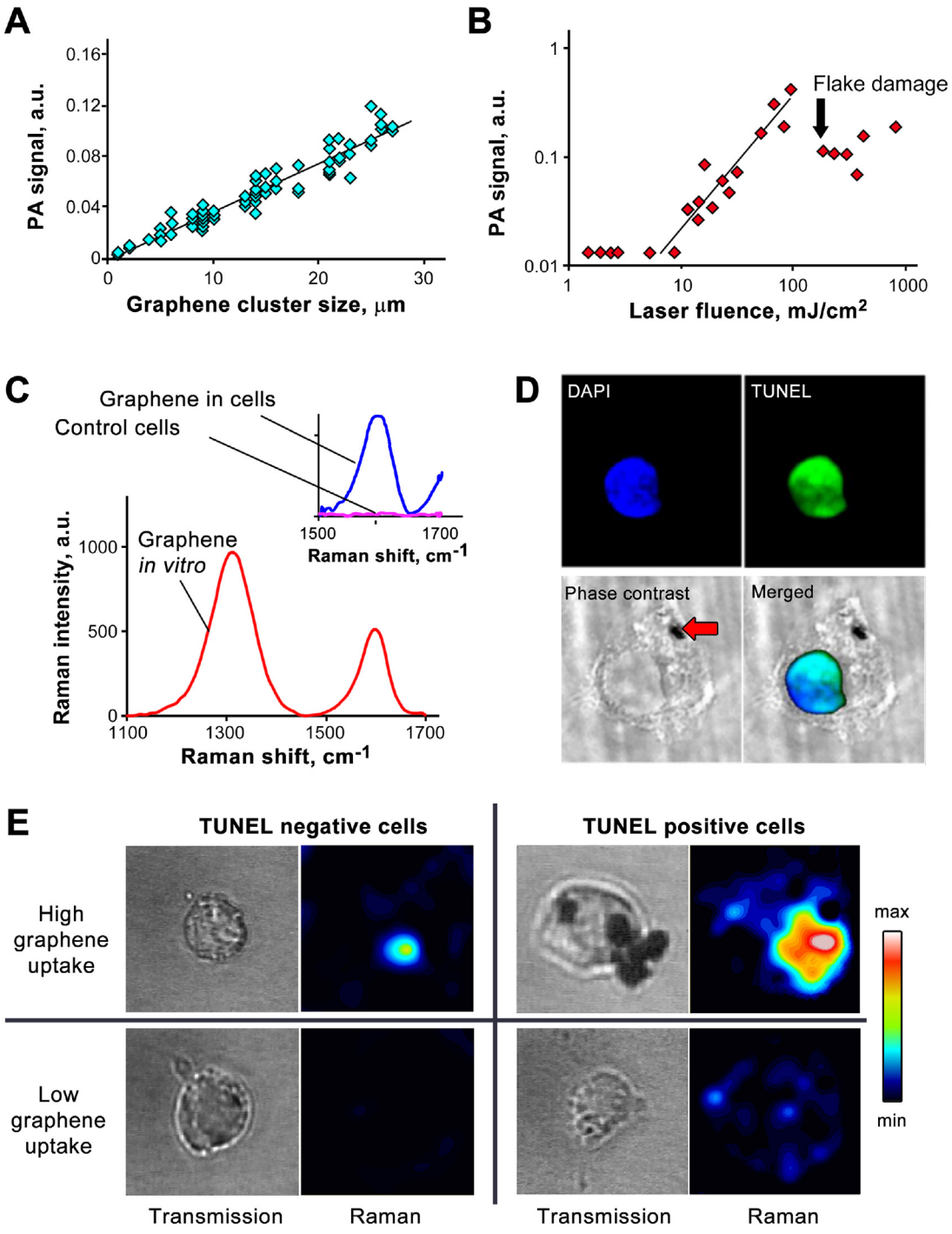

Fig. 5. PA and Raman label-free spectromicroscopy of graphene. A) PA signal calibration for clusters of different sizes. Dash indicates detection limit (PA signal of PBS + triple standard deviation). B) PA signal calibration for different laser energy levels. PA microscope parameters (panel A): 1064 nm, 50 mJ/cm^2, averaging of 50 PA signals, beam spot size 20 μm. For panel B, laser fluence: 1–1000 mJ/cm^2. C) Raman spectrum of control cells (no graphene) and graphene-incubated cells; D) Typical fluorescence imaging of a TUNEL-positive cell. The arrow indicates a visible cluster of graphene. E) Typical Raman images of graphene in TUNEL-positive and TUNEL-negative cells.

imaging GNRs bound to the cell membrane (Fig. 3A) using enhanced dark-field microscopy (CytoViva system). In some cases, using a library of typical GNR images to observe the scattering contrast of GNRs is sufficient for identification of NPs at the cell surface; however, the risk of false positive NP identification among control cells is very high. Small GNRs (25×113 nm) have low scattering contrast compared to cell structures. Here, non-fluorescent GNRs were selected to ensure full biocompatibility of the NPs to allow future development of *in vivo* detection methods for circulating tumor cells [24].

The PA detection of individual GNRs was demonstrated by analyzing extra-diluted NP solutions (10^6 particles/mL), assuming the low probability that multiple particles would be simultaneously present in the detection volume. Transient PA signals exceeding the threshold set up using the deionized water control were identified as individual particles. A four-fold increase in laser fluence of the pulsed laser did increase the amplitude of signals but did not increase the average particle count (particles/min), proving detection of all the particles in flow (single particle detection sensitivity). The amplitudes of the PA signals had normal distribution, while the intensity of the fluorescence signals was at the level of electronic noise of the detection system (Fig. 3B). We also observed the presence of high amplitude PA signals. Such signals were associated with clustering of GNRs since the relative number of the signals was not reduced by the additional dilution of the samples. The number of NP clusters was lower in nonreactive polymer-coated GNRs than in NPs with attached targeting moieties. On average, the number of clustered particles (particles above a horizontal threshold, Fig. 3B) was estimated to be in the range of 2–4%, even for fresh (5–7 weeks after synthesis) samples of antibody-conjugated GNRs. We estimated that the likelihood that two particles were randomly distributed into the same detection volume ($100 \times 100 \times 5$ μm or 0.05 nL) was 0.2% for 10^6 particles/mL (1 particle per 20 detection volumes) and 0.002% for 10^5 particles/mL solution (1 particle per 200 detection volumes).

To assess the efficacy of targeting breast cancer cells with GNRs covered with anti-EpCAM and anti-folate antibodies, we counted the number of cells with PA signals exceeding that of the control (unlabeled cells). Incubation of the breast cancer cells with the GNRs resulted in a dramatic increase in PA signal amplitude for the cells (up to 2 orders of magnitude). For both MDA-231-MB-GFP and ZR-75-1 cell lines, PAFFC provided simple and rapid quantification of NP-loaded cells. As many as 10^3 cells were analyzed in each experiment in less than 4 min. As expected, the ZR-75-1 cell line had somewhat higher EpCAM and lower folate expression compared to the MDA-231-MB-GFP cell line [47]. Labeling of these cells by a cocktail of anti-folate and anti-EpCAM GNRs minimized the differences in expression, resulting in similar labeling efficacy for both cell lines (Fig. 3C). The use of 2D PAFFC plots (Fig. 3D) simplified data analysis similarly to conventional flow cytometry charts. Here, the vertical threshold separated cells with high fluorescence from debris (low fluorescence). The horizontal threshold (PA signal) was set up using a negative control (cells only) and revealed the number of cells having GNRs normalized to all the cells (objects with high fluorescence). Simple comparison of the signal amplitudes, identification of the regions of interest, and post-experiment analysis of the results were based on recorded PA and fluorescence signal traces for each object (Fig. 3D, inset).

3.2. Analysis of nanomaterial toxicity

Multimodal PA-fluorescence cell analysis provides a unique opportunity to correlate expressions of cell biomarkers (including markers of cell damage and death) with the presence and quantity of nanoparticles on a cell-by-cell basis. The direct link to the presence of NPs may reveal damage mechanisms and ensure that the effects are related to the NPs and not to the unbound components [48]. Here, the PAFFC platform was used to analyze NRK-52E cells (rat kidney tubular epithelial cells) incubated with flakes of graphene for 24 h. Graphene has intrinsic light absorption contrast (providing PA detection), while TUNEL staining was used to identify nuclear DNA fragmentation (as a marker of irreversible cell death). A negative control (cells not exposed to graphene) and a positive control (cisplatin 80 μM, serum-free medium) were used to set up thresholds for PA (horizontal line) and fluorescence (vertical line) detection, respectively (Fig. 4A). 2D PAFFC scatter plots revealed a dramatic increase in absorbance for some cells, confirming the presence of graphene. The correlation between TUNEL intensity and the presence of graphene (Fig. 4A) was made based on comparison of graphene uptake and TUNEL intensity for single cells; the relative fraction of damaged cells was significantly higher for graphene concentrations exceeding 12 μg/mL (Fig. 4B). PAFFC data was not reported here for the 50 μg/mL graphene concentration due to the presence of significant amounts of unwashed graphene that interfered with the quantification of cell-bound nanomaterials.

Finally, PAFFC data was used to calculate the number of cells containing graphene after incubation. Two thresholds were selected (Fig. 4A, bottom right plot): one to identify cells with at least some graphene (PA signal of 0.004 a.u, lower blue line) and one—25-fold higher (0.1 a.u.)—to show only cells with high uptake (upper blue line). PAFFC data revealed that the relative number of cells having some graphene load was almost constant (Fig. 4C), *i.e.*, some nanomaterial quickly adhered to the cell surface. At the same time, the number of cells with a high graphene load was proportional to the total concentration of NPs during incubation (Fig. 4D).

The PA contrast of graphene is based on its sheets' intrinsic absorption of light. In order to estimate the sensitivity of the detection in flow, we measured PA signals for graphene clusters of different sizes resting on a glass surface (no flow), using transmission imaging for navigation and to estimate the dimensions of the graphene clusters. In general, the PA signal calibration curve was linear (Fig. 5A) for clusters smaller than the beam size (cluster size below 20 μm). The limit of detection at 50 mJ/cm2 laser fluence corresponded to a cluster with a diameter of 1 μm (Fig. 5A). At a higher laser fluence of 200 mJ/cm^2 (1064 nm excitation), the limit of detection corresponded to a cluster with a diameter of 0.2 μm. Further increase in laser fluence resulted in initial nonlinear amplification of the PA signal but led to flake damage (Fig. 5B).

In order to confirm PAFFC data on the presence of graphene in both healthy and damaged cells, we performed label-free Raman spectral identification (Figs. 5 C and S3) and imaging of graphene in TUNEL-positive (Fig. 5D) and negative cells, which were sorted using conventional FC. Spectral signatures of graphene in the Raman spectra provided reliable identification of the NPs in the complex biological background. Intensity of the G band of the graphene spectrum (1500–1700 cm^{-1}), integrated over the whole cell area, was used to quantify uptake for each cell. Measurements in control samples provided no graphene-specific Raman signatures, while samples incubated with graphene provided clear indication of NP accumulation (Fig. 5E). Raman microscopy confirmed the PAFFC data, showing that both TUNEL-positive and negative cells contained graphene. This correlated well with PA data (Fig. 4A) that showed the presence of TUNEL-negative cells with a significant graphene load. Raman imaging also confirmed that graphene was mostly bound to cell membranes; however, free-floating graphene particles were also seen.

4. Discussion

The integration of absorption-based PA detection with conventional FC instrumentation extends the range of possible FC applications to include non-fluorescent nanoparticles, pigments, and chromophores. With this integrated system, we have demonstrated rapid and simple screening of cancer cell labeling efficacy by targeted nanoparticles and analysis of nanoparticle toxicity. Other applications of the PAFFC technique may include detection of rare pigmented cancer cells *in vitro* using intrinsic cell pigmentation as an additional malignant cell marker (melanoma circulating tumor cells), analysis of nonspecific NP uptake, selection of optimal NP-antibody conjugates for cancer cell screening, and more. In contrast to conventional FC analysis, the proposed technology allows for the separation of changes in cell biomarker expression caused by NPs from those associated with unbound components, such as surfactants (*e.g.* CTAB) [48], heavy metal ions (*e.g.* Ag+) [49], and other contaminants of NP formulations [50]. For the majority of non-fluorescent NPs, quantification of uptake is complex and requires extensive resources. For some materials, like graphene (mostly pure carbon atoms), no rapid quantification techniques currently exist, while any material modifications (*e.g.* fluorescent tags) will eventually change NP properties.

As demonstrated here, the PA system provides detection of single GNRs with negligible background absorption from the cells. Light scattering contrast of NPs was previously used for quantification of NPs in some FC applications; however, significant light scattering by cell structures (Fig. 3A) limits the use of this method to large particles or large aggregates consisting of multiple NPs. Raman spectral identification (demonstrated here for graphene) can be applied to a variety of materials; however, it lacks speed and, hence, is limited to slow flows [25]. The high throughput (5–10 min/sample) of PAFFC is essential for screening large cell populations and analyzing multiple experimental parameters to achieve accurate optimization of cell-NP interactions. Here, we demonstrated that PA detection can be used for the optimization of molecule-specific cell targeting by NPs and the identification of the most specific and efficient antibody-NP conjugates. It is also possible to use PAFFC for analysis of healthy blood and endothelial cell interactions with NPs in order to predict the extent of nonspecific targeting *in vivo*. The multimodal cell analysis (fluorescence, light scattering, absorption) provides unique data that could be used for understanding the mechanisms of NP-cell interactions. Our PA data on graphene uptake (Fig. 4A, right bottom panel) highlighted that not all the cells containing graphene were damaged. This could be related to the inability of PAFFC to distinguish between multiple single flakes (which have a higher chance of penetrating into a cell) and large clusters of graphene on a cell surface, or with cell damage by very small flakes not being detectable by the current PAFFC system. Raman imaging has partially confirmed these findings: some TUNEL-positive cells exhibited very low graphene uptake (Fig. 5E, bottom right panel), and some TUNEL-negative cells featured large graphene particles (Fig. 5E, top left panel).

Characterization of cells based on the presence of NPs is demonstrated here; however, much remains to be done to increase the accuracy of NP quantification using the PA technique. Among the major hurdles are the absence of standard materials for calibration and the nonlinear phenomena that enhance PA signals [36]. We have previously demonstrated the use of dual contrast magnetic beads for calibration of PAFFC; [37] however, such beads cannot accurately represent a cell with NPs. We believe that calibration can be performed using polymer-nanoparticle composite beads with embedded NPs (*e.g.* gold nanospheres). Nonlinear phenomena may also result in cell damage by heat, acoustic pressure, or through formation of nano-sized bubbles around over-heated NPs. These effects may affect cell viability during analysis and, thus, have to be taken into consideration. Calibration of PA detection under static conditions (no flow, Fig. 5A) allows sensitivity estimation; however, the development of reliable reference standard materials is essential for reliable quantitative analysis.

The sensitivity of PA detection can be improved through better matching frequency of the ultrasound transducer to the frequency of the PA signal collected from the sample. In linear heating mode, NPs generate acoustic signals in the GHz frequency range; [51] thus, 20 MHz detection frequency may not be optimal. However, acoustic attenuation by quartz capillary and the layer of water dramatically reduce the high-frequency component of the signal, decreasing the sensitivity gains for high-frequency detectors. Here, we did not analyze the possibility of increasing detection sensitivity through the use of a higher frequency detector. However, a transducer placed closer to the sample and elimination of a quartz capillary from the acoustic wave path may prevent losses of high frequency ultrasound energy to increase detection sensitivity. This will be tested in our future research.

Finally, the PAFFC design presented here can be potentially improved by eliminating the water used for acoustic coupling between the flow cell and ultrasound transducer. Water coupling complicates system maintenance and limits optical access to the cell. There is no actual need for water-coupling, as direct contact between transducer and flow cell would suffice for PA detection, as we previously demonstrated in glass tubes [35]. Such water-free coupling based on a solid contact would simplify the integration of PA detection into existing FC instrumentation, without compromising detection sensitivity or performance of conventional detection.

5. Conclusions

We have demonstrated that high-speed PA detection can be easily incorporated into existing flow cytometry schematics for label-free quantification of non-fluorescent nanoparticles, as well as light absorbing proteins and dye molecules. The major advantages of our PAFFC system are its high throughput, single particle sensitivity, and label-free detection of non-fluorescent particles. PA detection is proposed not as a replacement of fluorescence, but as an additional modality that can expand the range of applications for conventional flow cytometry, especially in the field of nanotoxicology, where information on uptake quantification by individual cells may shed light on cell-nanoparticle interactions.

Conflict of interest

The authors declare that there are no conflicts of interest.

Acknowledgements

This work was supported by grants from the National Institute of Health (R01CA131164, R01EB009230, R01EB017217, P20GM109005, R21EB0005123, and R21CA139373), the National Science Foundation (DBI-0852737), the award from the Department of Health and Human Services, DoD TATRC program, and VA Merit Review (I01 BX002425-01), as well as grants from the Pepper Center, the Arkansas Bioscience Institute, and the Translational Research Institute at the University of Arkansas for Medical Sciences. Partial funding for equipment/facilities used in this research was provided by the Center for Advanced Surface Engineering, under the National Science Foundation Grant No. IIA-1457888 and the Arkansas EPSCoR Program, ASSET III. This

work was also supported by the U.S. Food and Drug Administration (award HHSF223201210189C administered through Arkansas Research Alliance). The views presented in this paper are not necessarily those of the U.S. FDA.

We also acknowledge Emily Davis for help with editing this manuscript.

Appendix A. Supplementary data

Supplementary data associated with this article can be found, in the online version, at http://dx.doi.org/10.1016/j.pacs.2017.03.002.

References

[1] A. Gojova, B. Guo, R.S. Kota, J.C. Rutledge, I.M. Kennedy, A.I. Barakat, Induction of inflammation in vascular endothelial cells by metal oxide nanoparticles: effect of particle composition, Environ. Health Perspect. 115 (2007) 403–409.
[2] P. Nativo, I.A. Prior, M. Brust, Uptake and intracellular fate of surface-modified gold nanoparticles, ACS Nano 2 (2008) 1639–1644.
[3] C.C. Fleischer, C.K. Payne, Nanoparticle-cell interactions molecular structure of the protein corona and cellular outcomes, Acc. Chem. Res. 47 (2014) 2651–2659.
[4] L. Shang, K. Nienhaus, G.U. Nienhaus, Engineered nanoparticles interacting with cells: size matters, J. Nanobiotechnol. 12 (2014).
[5] A. Verma, F. Stellacci, Effect of surface properties on nanoparticle-cell interactions, Small (Weinheim an der Bergstrasse, Germany) 6 (2010) 12–21.
[6] R. Coradeghini, S. Gioria, C.P. Garcia, P. Nativo, F. Franchini, D. Gilliland, J. Ponti, F. Rossi, Size-dependent toxicity and cell interaction mechanisms of gold nanoparticles on mouse fibroblasts, Toxicol. Lett. 217 (2013) 205–216.
[7] S. Tatur, M. Maccarini, R. Barker, A. Nelson, G. Fragneto, Effect of functionalized gold nanoparticles on floating lipid bilayers, Langmuir 29 (2013) 6606–6614.
[8] K. Bhattacharyya, B.S. Goldschmidt, M. Hannink, S. Alexander, A. Jurkevic, J.A. Viator, Gold nanoparticle–mediated detection of circulating cancer cells, Clin. Lab. Med. 32 (2012) 89–101.
[9] K.E. Scarberry, R. Mezencev, J.F. McDonald, Targeted removal of migratory tumor cells by functionalized magnetic nanoparticles impedes metastasis and tumor progression, Nanomedicine (London, England) 6 (2011) 69–78.
[10] B. Faltas, Cornering metastases: therapeutic targeting of circulating tumor cells and stem cells, Front. Oncol. 2 (2012) 68.
[11] E.I. Galanzha, V.P. Zharov, Photoacoustic flow cytometry, Methods (San Diego, Calif.) 57 (2012) 280–296.
[12] Z.A. Nima, M. Mahmood, Y. Xu, T. Mustafa, F. Watanabe, D.A. Nedosekin, M.A. Juratli, T. Fahmi, E.I. Galanzha, J.P. Nolan, A.G. Basnakian, V.P. Zharov, A.S. Biris, Circulating tumor cell identification by functionalized silver-gold nanorods with multicolor, super-enhanced SERS and photothermal resonances, Sci. Rep.-UK 4 (2014).
[13] J. Xie, Y. Lu, H. Dong, R. Zhao, H. Chen, W. Shen, P.J. Sinko, Y. Zhu, J. Wang, J. Shao, Y. Gao, F. Xie, L. Jia, Enhanced specificity in capturing and restraining circulating tumor cells with dual antibody–dendrimer conjugates, Adv. Funct. Mater. (2015) n/a–n/a.
[14] A. Elsaesser, A. Taylor, G.S. de Yanes, G. McKerr, E.M. Kim, E. O'Hare, C.V. Howard, Quantification of nanoparticle uptake by cells using microscopical and analytical techniques, Nanomedicine (London, England) 5 (2010) 1447–1457.
[15] Y. Ibuki, T. Toyooka, Nanoparticle uptake measured by flow cytometry, Methods Mol. Biol. (Clifton, N.J.) 926 (2012) 157–166.
[16] S. Klein, S. Petersen, U. Taylor, D. Rath, S. Barcikowski, Quantitative visualization of colloidal and intracellular gold nanoparticles by confocal microscopy, J. Biomed. Opt. 15 (2010).
[17] M.J. Crow, S.M. Marinakos, J.M. Cook, A. Chilkoti, A. Wax, Plasmonic flow cytometry by immunolabeled nanorods, Cytom. Part A 79A (2011) 57–65.
[18] C. Muhlfeld, T.M. Mayhew, P. Gehr, B. Rothen-Rutishauser, A novel quantitative method for analyzing the distributions of nanoparticles between different tissue and intracellular compartments, J. Aerosol Med. 20 (2007) 395–407.
[19] B.D. Chithrani, A.A. Ghazani, W.C.W. Chan, Determining the size and shape dependence of gold nanoparticle uptake into mammalian cells, Nano Lett. 6 (2006) 662–668.
[20] C. Gottstein, G. Wu, B.J. Wong, J.A. Zasadzinski, Precise quantification of nanoparticle internalization, ACS Nano 7 (2013) 4933–4945.
[21] S.R. Abulateefeh, S.G. Spain, K.J. Thurecht, J.W. Aylott, W.C. Chan, M.C. Garnett, C. Alexander, Enhanced uptake of nanoparticle drug carriers via a thermoresponsive shell enhances cytotoxicity in a cancer cell line, Biomater. Sci. 1 (2013) 434–442.
[22] A.P. Alivisatos, W.W. Gu, C. Larabell, Quantum dots as cellular probes, Annu. Rev. Biomed. Eng. 7 (2005) 55–76.
[23] M. Huang, Z.S. Ma, E. Khor, L.Y. Lim, Uptake of FITC-chitosan nanoparticles by a549 cells, Pharm. Res. 19 (2002) 1488–1494.
[24] H.M. Shapiro, Practical Flow Cytometry, Wiley, 2003.
[25] J.P. Nolan, D.S. Sebba, Surface-enhanced Raman scattering (SERS) cytometry, Methods Cell Biol. 102 (2011) 515–532.
[26] A. Kumar, A.K. Pandey, S.S. Singh, R. Shanker, A. Dhawan, A flow cytometric method to assess nanoparticle uptake in bacteria, Cytom. Part A 79A (2011) 707–712.
[27] R.M. Zucker, E.J. Massaro, K.M. Sanders, L.L. Degn, W.K. Boyes, Detection of TiO2 nanoparticles in cells by flow cytometry, Cytom. Part A 77A (2010) 677–685.
[28] M.A. van Dijk, A.L. Tchebotareva, M. Orrit, M. Lippitz, S. Berciaud, D. Lasne, L. Cognet, B. Lounis, Absorption and scattering microscopy of single metal nanoparticles, Phys. Chem. Chem. Phys. 8 (2006) 3486–3495.
[29] X. Wu, F. Tian, W. Wang, J. Chen, M. Wu, J.X. Zhao, Fabrication of highly fluorescent graphene quantum dots using l-glutamic acid for in vitro/in vivo imaging and sensing, J. Mater. Chem. C 1 (2013) 4676–4684.
[30] S.Y. Emelianov, P.-C. Li, M. O'Donnell, Photoacoustics for molecular imaging and therapy, Phys. Today 62 (2009) 34–39.
[31] L.V. Wang, Multiscale photoacoustic microscopy and computed tomography, Nat. Photonics 3 (2009) 503–509.
[32] H.F. Zhang, K. Maslov, G. Stoica, L.V. Wang, Functional photoacoustic microscopy for high-resolution and noninvasive in vivo imaging, Nat. Biotechnol. 24 (2006) 848–851.
[33] L.V. Wang, Prospects of photoacoustic tomography, Med. Phys. 35 (2008) 5758–5767.
[34] E.I. Galanzha, E.V. Shashkov, P.M. Spring, J.Y. Suen, V.P. Zharov, In vivo, noninvasive, label-free detection and eradication of circulating metastatic melanoma cells using two-color photoacoustic flow cytometry with a diode laser, Cancer Res. 69 (2009) 7926–7934.
[35] D.A. Nedosekin, M. Sarimollaoglu, E.V. Shashkov, E.I. Galanzha, V.P. Zharov, Ultra-fast photoacoustic flow cytometry with a 0.5 MHz pulse repetition rate nanosecond laser, Opt. Express 18 (2010) 8605–8620.
[36] V.P. Zharov, Ultrasharp nonlinear photothermal and photoacoustic resonances and holes beyond the spectral limit, Nat. Photon. 5 (2011) 110–116.
[37] D.A. Nedosekin, M. Sarimollaoglu, E.I. Galanzha, R. Sawant, V.P. Torchilin, V.V. Verkhusha, J. Ma, M.H. Frank, A.S. Biris, V.P. Zharov, Synergy of photoacoustic and fluorescence flow cytometry of circulating cells with negative and positive contrasts, J. Biophotonics 6 (2013) 425–434.
[38] D.A. Nedosekin, E.I. Galanzha, E. Dervishi, A.S. Biris, V.P. Zharov, Super-resolution nonlinear photothermal microscopy, Small (Weinheim an der Bergstrasse Germany) 10 (2014) 135–142.
[39] S. Mallidi, T. Larson, J. Tam, P.P. Joshi, A. Karpiouk, K. Sokolov, S. Emelianov, Multiwavelength photoacoustic imaging and plasmon resonance coupling of gold nanoparticles for selective detection of cancer, Nano Lett. 9 (2009) 2825–2831.
[40] V.P. Zharov, E.I. Galanzha, E.V. Shashkov, N.G. Khlebtsov, V.V. Tuchin, In vivo photoacoustic flow cytometry for monitoring of circulating single cancer cells and contrast agents, Opt. Lett. 31 (2006) 3623–3625.
[41] J.A. Viator, M.J. Sims, T.S. Thomas, P.S. Dale, A.E. Lisle, U. Atasoy, Photoacoustic detection of gold nanoparticle enhanced circulating breast cancer cells, Lasers Surg. Med. 3–3 (2008).
[42] E.I. Galanzha, E.V. Shashkov, V.V. Tuchin, V.P. Zharov, In vivo multispectral, multiparameter, photoacoustic lymph flow cytometry with natural cell focusing, label-free detection and multicolor nanoparticle probes, Cytom. Part A 73 (2008) 884–894.
[43] D.A. Nedosekin, M.V. Khodakovskaya, A.S. Biris, D. Wang, Y. Xu, H. Villagarcia, E.I. Galanzha, V.P. Zharov, In vivo plant flow cytometry: a first proof-of-concept, Cytome. Part A 79 (2011) 855–865.
[44] J.A. Viator, S. Gupta, B.S. Goldschmidt, K. Bhattacharyya, R. Kannan, R. Shukla, P. S. Dale, E. Boote, K. Katti, Gold nanoparticle mediated detection of prostate cancer cells using photoacoustic flowmetry with optical reflectance, J. Biomed. Nanotechnol. 6 (2010) 187–191.
[45] G. Gutierrez-Juarez, S.K. Gupta, R.M. Weight, L. Polo-Parada, C. Papagiorgio, J.D. Bunch, J.A. Viator, Optical photoacoustic detection of circulating melanoma cells In vitro, Int. J. Thermophys. 31 (2010) 784–792.
[46] Y. Wang, K. Maslov, Y. Zhang, S. Hu, L. Yang, Y. Xia, J. Liu, L.V. Wang, Fiber-laser-based photoacoustic microscopy and melanoma cell detection, J. Biomed. Opt. 16 (2011) 011014.
[47] E.A. Punnoose, S.K. Atwal, J.M. Spoerke, H. Savage, A. Pandita, R.F. Yeh, A. Pirzkall, B.M. Fine, L.C. Amler, D.S. Chen, M.R. Lackner, Molecular biomarker analyses using circulating tumor cells, PLoS One 5 (2010).
[48] A.M. Alkilany, P.K. Nagaria, C.R. Hexel, T.J. Shaw, C.J. Murphy, M.D. Wyatt, Cellular uptake and cytotoxicity of gold nanorods: molecular origin of cytotoxicity and surface effects, Small (Weinheim an der Bergstrasse, Germany) 5 (2009) 701–708.
[49] C. Beer, R. Foldbjerg, Y. Hayashi, D.S. Sutherland, H. Autrup, Toxicity of silver nanoparticles—nanoparticle or silver ion? Toxicol. Lett. 208 (2012) 286–292.
[50] H. Vallhov, J. Qin, S.M. Johansson, N. Ahlborg, M.A. Muhammed, A. Scheynius, S. Gabrielsson, The importance of an endotoxin-free environment during the production of nanoparticles used in medical applications, Nano Lett. 6 (2006) 1682–1686.
[51] A. Prost, F. Poisson, E. Bossy, Photoacoustic generation by a gold nanosphere: from linear to nonlinear thermoelastics in the long-pulse illumination regime, Phys. Rev. B 92 (2015).

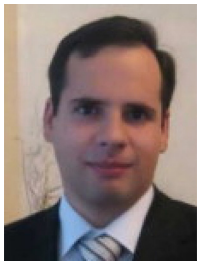

Dmitry Nedosekin, PhD, is a Research Associate at the Phillips Classic Laser & Nanomedicine Laboratories, University of Arkansas for Medical Sciences. He completed doctoral training at the Philipps-Universität Marburg, Germany (2004–2005) and at the M.V. Lomonosov Moscow State University, Russia (2003–2007) and received a Ph.D. degree on Analytical Chemistry. His scientific interests cover a wide range of biophotonic methods including the development of instrumentation that integrates fluorescence, photothermal, photoacoustic, and Raman spectroscopy techniques for biomedical imaging and in-flow analysis.

Tariq Fahmi MD, PhD, is a Research Associate at Department of Pharmacology and Toxicology, University of Arkansas for Medical Sciences. He received his medical degree in Medicine and General Surgery from the Medical College/Al-Mustansiriya University, Baghdad, and MSc. in pathology from the Medical college/Al-Nahrain University, Baghdad, Iraq, and Ph.D. degree in Oncology from Haccettepe University, Ankara, Turkey.H is research experience includes pathology, molecular biology, toxicology and assay development.

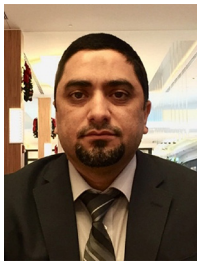

Zeid A. Nima, PhD, is Postdoctoral – Research Fellow, University of Arkansas at Little Rock, Center for integrative Nanotechnology Sciences. He received his B.Sc. and M.Sc. in Instrumental chemical analysis from University of Baghdad, Baghdad, Iraq, and M.Sc. in Applied sciences and Ph.D. in Applied sciences emphasis in Applied Chemistry from University of Arkansas at Little Rock, Little Rock, AR, USA. His research experience includes: Various spectroscopic analytical techniques: Raman Spectroscopy, Surface Enhanced Raman Spectroscopy (SERS), UV–vis spectroscopy, FT-IR spectroscopy, ICP-MS spectroscopy, Atomic Absorption spectroscopy, Fluorescence spectroscopy, and Luminescence spectroscopy, Microscopic imaging techniques: Microscope, Fluorescence Microscope, Scanning Electron Microscopy (SEM), Transmission Electron Microscope (TEM), Atomic Force Microscope (AFM), Thermal Gravimetric Analysis (TGA), XRD and XPS., Synthesis and characterization of plasmonically active nanomaterials, Functionalization of different shapes and sizes of nanomaterials with bio-active molecules including proteins, antibodies, drugs, and photoactive biomolecules, Functionalization of carbon-based nanomaterials (Carbon nanotubes and Graphene) with various types of biomolecules, Use of specifically designed nanomaterials to detect and identify single cancer tumor cells (CTCs) in blood and other biological fluids, Analytical techniques such as HPLC, GC–MS, and TLC Chromatography.

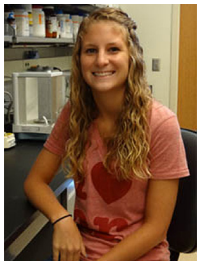

Jacqueline Nolan, is a graduate student at the Philips Classic Laser & Nanomedicine Laboratories, University of Arkansas for Medical Sciences. She received her B.S. degree in Biology from the University of Arkansas-Fayetteville. Her current research project involves using a novel multimodal in vivo flow cytometry system to understand the role of anti-cancer drugs on the viability of circulating tumor cells.

Chengzhong Cai, MD, PhD, is previously a Research Assistant at the Phillips Classic Laser & Nanomedicine Laboratories, University of Arkansas for Medical Sciences. He received his M.D. degrees from Medical school of Tong-ji University in China, and Ph.D. degree from Philipps-University Marburg in Germany. His research experience includes the development of high-speed photoacoustic flow cytometry systems, cancer growth and metastasis in head and neck, drug induced toxicity in human body.

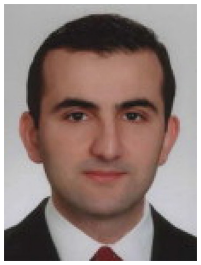

Mustafa Sarimollaoglu, PhD, is a research associate at the Arkansas Nanomedicine Center, University of Arkansas for Medical Sciences. He received his B.S. and M.S degrees in electronics and communication engineering from Istanbul Technical University, Turkey, and Ph.D. degree in integrated computing at the University of Arkansas at Little Rock, the USA. His research experience includes the development of high-speed photoacoustic flow cytometry systems, image and signal processing in biomedicine.

Enkeleda Dervishi, PhD, received her B.S. in Electronic and Computer Engineering Technology and her Ph.D. degree in Engineering Science and Systems from the University of Arkansas at Little Rock (UALR). In 2013, Enkeleda joined the Center for Integrated Nanotechnologies and Materials Physics and Application Division at the Los Alamos National Laboratory as a Marie Curie Distinguished Postdoctoral Fellow, and is currently a staff scientist. Her research is focused on synthesis of unique multi-functional heterostructures for a number of applications ranging from energy storage to sensors and nanoelectronics. Enkeleda has authored/coauthored over eighty publications in peer reviewed journals and she is currently a reviewer and on the editorial board for a number of international journals.

Alexei Basnakian, PhD, DSc, received his PhD and DSc degrees from the Russian Academy of Medical Science, both in the field of DNases. He had postdoctoral trainings in molecular biology at the Harvard Medical School and in toxicology/cancer research at the National Center for Toxicological Research/FDA. Dr. Basnakian is a Professor in the Department of Pharmacology and Toxicology, and Director of the DNA Damage and Toxicology Core Center at the University of Arkansas for Medical Sciences, and Research Career Scientist at the Central Arkansas Veterans Healthcare System. He is an author of more than 85 peer-reviewed papers and 12 reviews or book chapters. Dr. Basnakian is an Editorial Board member of four biomedical journals, and a member of NIH and VA grant study sections. His research interests are in DNA endonucleases and DNA damage associated with toxicity, anti-cancer therapy, cell injury and cell death.

Alexandru Biris, PhD, leads the research at the Center for Integrative Nanotechnology Sciences, at the University of Arkansas at Little Rock exploring the science of nanostructures that can be used to alter the properties of other substances at the atomic level. Dr. Biris serves as Director and Chief Scientist to accelerate the development of applications of nanotechnology. Dr. Biris is also Professor at the Systems Engineering Department at the Donaghey College of Engineering and Information Technology and is the Sturgis Endowed Chair for Excellence in Nano-Sciences. His areas of expertise include Nanotechnology, Raman Spectroscopy and X-Ray Diffraction, Planetary Instrumentation (Mars Dust Analyzer), Particulate Science, Nanoparticle and Carbon Nanotube Generation, Nanomedicine, Nanocomposite Materials for Space Exploration, Surface Technology, Nano-Sensors

and Bio Nano-Sensors, Materials Science and Engineering, Coating Technology, Hydrogen Interaction with Metals, Alloys, and Carbon Nanostructures *etc*.

Vladimir P. Zharov, PhD, DSc, is the director of the Arkansas Nanomedicine Center, a Professor of Biomedical Engineering (BME) and Josephine T. McGill Chair in Cancer Research at the University of Arkansas for Medical Sciences (UAMS), the USA. He received his Ph.D. and D.Sc. degrees from Bauman Moscow State Technical University (BMSTU), completed a postdoctoral fellowship at Lawrence Berkeley National Laboratory of the University of California and served as the Chairman of the BME department at BMSTU. He is the author of 5 books, 52 patents, and more than 200 papers in the field of laser spectroscopy, biophotonics, and nanomedicine including six publications in the Nature family journals. He is one of the pioneers of high resolution photoacoustic spectroscopy and the inventor of photoacoustic tweezers, pulse nanophotothermolysis of infections and cancer, and *in vivo* multicolor flow cytometry. Dr. Zharov is the principle investigator on 16 NIH (5R01), NSF, and other agency grants. His laser-based technologies have been commercialized and used in clinics. Dr. Zharov is the State Prize Winner in Russia, the most prestigious national award in Russia, and the first recipient of the U.S. Maiman Award named after the inventor of the first laser.